1709

Université de Neuchâtel
Institut de Physique

Photoemissionsstudie eindimensionaler Metallketten

Travail de thèse présenté à l'Institut de Physique de l'Université de Neuchâtel pour l'obtention du grade de Docteur ès Sciences

Oliver Gallus

Neuchâtel, 2003

Forme réduite de la thèse pour l'obtention du grade de Docteur ès Sciences de l'Université de Neuchâtel

IMPRIMATUR POUR LA THESE

Photoemissionsstudie eindimensionaler Metallketten

de M. Oliver GALLUS

UNIVERSITE DE NEUCHATEL

FACULTE DES SCIENCES

La Faculté des sciences de l'Université de Neuchâtel, sur le rapport des membres du jury

MM. Y. Baer (directeur de thèse),
P. Aebi et W.-D. Schneider (Lausanne)

autorise l'impression de la présente thèse.

Neuchâtel, le 2 juillet 2003

Le doyen:

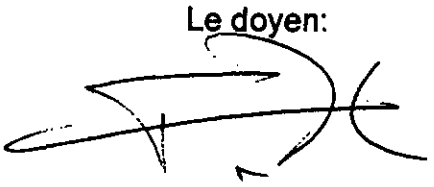

François Zwahlen

Les publications listées dans la table des matières ci-dessous représentent une forme réduite de la thèse pour l'obtention du grade de Docteur ès Sciences de l'Université de Neuchâtel

Table des matières

[1] O. Gallus, Th. Pillo, M. Hengsberger, P. Segovia, and Y. Baer, *A system with a complex phase transition: Indium chains on Si(111)*, The European Physical Journal B **20**, 313 (2001).

[2] O. Gallus, Th. Pillo, P. Starowicz, and Y. Baer, *Honeycomb chain-channel (HCC) signature in the calcium-induced Si(111)-(3×2) surface*, Europhysics Letters **60**, 903 (2002).

[3] P. Starowicz, O. Gallus, Th. Pillo, and Y. Baer, *Size Effects in Photoemission of One-Dimensional Metals*, Physical Review Letters **89**, 256402 (2002).

Le texte complet de la thèse est déposé à la bibliothèque de la section de Physique de la faculté des Sciences de l'Université de Neuchâtel et au Service des bibliothèques de l'Université de Neuchâtel.

Le texte complet est rédigé en allemand.

Publication [1]

O. Gallus, Th. Pillo, M. Hengsberger, P. Segovia, and Y. Baer, *A system with a complex phase transition: Indium chains on Si(111)*, The European Physical Journal B **20**, 313 (2001).

Eur. Phys. J. B **20**, 313–319 (2001)

THE EUROPEAN PHYSICAL JOURNAL B

EDP Sciences

A system with a complex phase transition: Indium chains on Si(111)

O. Gallus, Th. Pillo[a], M. Hengsberger[b], P. Segovia, and Y. Baer

Institut de Physique, Université de Neuchâtel, rue A.-L. Breguet 1, 2000 Neuchâtel, Switzerland

Received 12 December 2000 and Received in final form 8 February 2001

Abstract. We examined in detail the geometric and electronic structure of thin In chains on vicinal Si(111) surfaces by means of low energy electron diffraction and ultrahigh-resolution photoemission as a function of temperature. Our data reveal a transition around $T_c = 115$ K from a high temperature (4 × 1)- to a low temperature (8 × 2)-phase being reversible with a small hysteresis of the order 10 K. ARPES spectra exhibit clearly important concomitant changes in the electronic band structure near the Fermi surfaces and at the border of the surface Brillouin zones. We derive the dispersive behavior of the bands involved in the transition in detail and demonstrate that at least two surface state bands m_2 and m_3 show the opening of a pseudo energy gap on the Fermi surface leaving small but finite spectral weight in the low-temperature state. We conclude that this transition is probably driven by a similar but more complex mechanism than in a conventional Peierls transition.

PACS. 71.30.+h Metal-insulator transitions and other electronic transitions – 71.45.Lr Charge-density-wave systems – 79.60.-i Photoemission and photoelectron spectra

1 Introduction

Low-dimensional materials exhibit a vast number of unconventional physical phenomena which have motivated numerous photoemission studies in the last decade [1] in order to investigate their electronic structure. When the dimensionality (D) of solids is reduced from 3D to 1D, the usual Fermi liquid description of correlated electrons breaks down and the familiar concept of quasiparticles is no longer existing. It must be replaced by the theoretical approach developed by Luttinger [2] establishing that only two types of collective excitations are existing, the holons and the spinons, which are separated and show different dispersions when moving away from the Fermi level E_F. Very recently, this theoretical picture has been explicitly observed with angle-resolved photoemission spectroscopy (ARPES) on a nearly ideal 1D system consisting of Au chains on a vicinal Si(111) surface [3]. However, in most real systems the transverse interaction between the chains is not negligible and is, hence, responsible for low-temperature phase transitions involving coherence in more than one dimension. Charge density waves (CDW) or spin density waves (SDW) are formed along the chains which can be concomitant with a periodic lattice distortion (PLD) in the former case [4,5]. Until now the observation of these mechanisms has been mainly limited to anisotropic solids with a pronounced 1D character, *e.g.* in inorganic salts or bronzes [1,6,7].

Recently, electron spectroscopic studies of self-assembling indium chains on Si(111) have been found to exhibit a metal-insulator transition at 130 K [8,9]. The Si(111)-(4 × 1)-In surface is well known among other In/Si surface reconstructions [10–18] and several attempts have been made to resolve in detail the surface geometric structure [19,20], but only very recently surface X-ray diffraction studies [21,22] could deduce the detailed geometric structure of the Si(111)-(4 × 1)-In surface. Numerous photoemission and inverse photoemission data are available [8,10,14,16,17] establishing finally the existence of three metallic bands [10]. From a single study using ARPES, RHEED, and STM [8] the existence of a phase transition has been demonstrated. Beyond the evidence of the pronounced 1D character of these bands and their important intensity reduction around E_F at low temperature, the detailed dispersion of these states and their temperature dependence through the transition has not been obtained.

Our aim in the present study is to extract from high-resolution ARPES spectra the detailed electronic band structure of the surface states involved in the phase transition and to relate their modification to the change of periodicity determined by LEED. We clearly observe this reversible transition at 115 K from the high-temperature (4 × 1)- to the low-temperature (8 × 2)-phase. Two metallic bands with sharp Fermi steps revealed by the

[a] e-mail: thorsten.pillo@unine.ch

[b] *Present address:* Physik-Institut, Universität Zürich, Winterthurerstr. 190, 8057 Zürich, Switzerland

photoemission spectra at high temperature are shifted to lower binding energies below the phase transition and a tiny intensity is left at the Fermi energy in the range of the high-temperature Fermi wave vectors. The dispersion of the bands and their evolution through the transition show a rather complex and unconventional behavior around the point X at the border of the first Brillouin zone (BZ). This anomalous situation can be qualitatively related to the accumulation of boundaries of higher BZs in this range, which are modified by the transition. The discussion of these results shows that the complexity of the mechanism driving the transition results from participation of more than one band.

2 Experiment

Indium chains were prepared on a Si(111) wafer (p-doped, $\rho \sim 5\ \Omega$cm), miscut by 1.1° in the $[\bar{1}\bar{1}2]$-direction to obtain a predominantly single domain growth of the chains. Prior to evaporation, the wafer (cut into a rectangle, $5 \times 19 \times 0.5$ mm^3) was cleaned by DC resistive heating along the chain direction to obtain well-ordered Si(111)-(7×7) surfaces as identified by low energy electron diffraction (LEED) [10]. The cleanness was further checked by X-ray photoelectron spectroscopy (XPS) and Auger spectroscopy (AES). After the cleaning ~1.2 Monolayers (ML) In, as determined from XPS, were evaporated by electron bombardment from a water-cooled Knudsen-cell-type evaporator onto the wafer held at room temperature. Subsequently, the In films were annealed (DC heating) up to 440° C for about 70 sec. This procedure resulted in well-ordered single domain Si(111)-(4×1)-In chains as shown in Figure 1b.

The electron spectrometer (SCIENTA SES-200) is equipped with a hemispherical electron analyser and two He discharge lamps, the angle between the incident light and the detector being fixed to ±45°. The photon source used here is connected to a double-focusing monochromator to produce highly linearly polarized light. All spectra presented in this study have been taken with p-polarized HeI-photons (21.2 eV, polarization vector in the measurement plane) and normalized to the measurement time. Photoelectrons are recorded by a two-dimensional detector with energy and angular resolution set to 5 meV and ±0.5°, respectively. By use of a flow cryostat, samples can readily be cooled down using either liquid helium or liquid nitrogen. The temperature is measured by a Pt resistance and can be controlled by resistive counter-heating with an accuracy of ±1 K. ARPES spectra were taken along the chain direction, *i.e.*, along the [ΓX]-azimuth of the 1st surface Brillouin zone (SBZ), as indicated in Figure 1a.

3 Results

Figure 1 shows in part (a) the SBZ of the (4 × 1) surface. The filled and empty circles display the Si(111) (1×1) and the In/Si (4 × 1) Γ-points, respectively. They are reflected in the LEED experiment shown in part (b) of Figure 1.

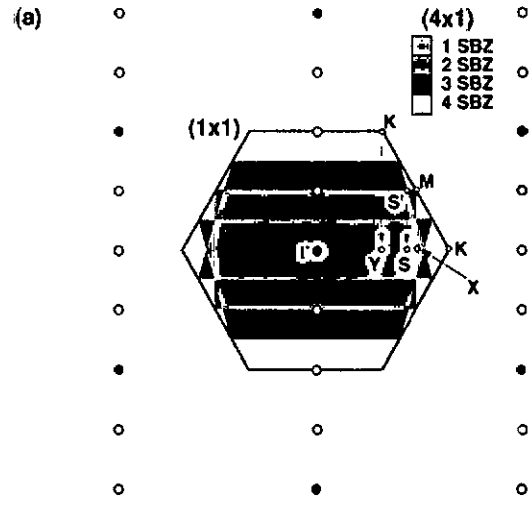

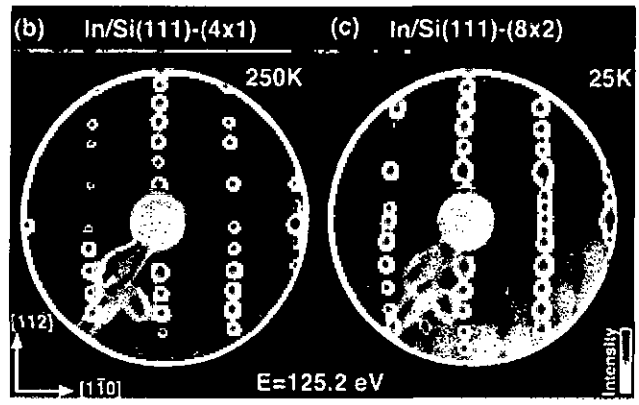

Fig. 1. (a) Sketch of the surface Brillouin zone (SBZ) of the Si(111)-(1×1) surface (hexagon) and the corresponding (4×1)-SBZ induced by the In overlayer (shown as rectangles and repeated in the extended zone scheme in the $[11\bar{2}]$-direction). High symmetry points are labeled. (b) LEED pattern of a single-domain Si(111)-(4 × 1)In surface, taken at 250 K with 125.2 eV electrons. Note the inverted grayscale with high intensity corresponding to black. (c) LEED pattern taken at 25 K. The change in surface symmetry is evident.

The large hexagon in part (a) is the SBZ of the (1 × 1) surface, whereas the small trapezoidal parts, displayed in different grayscales, show the 1st, 2nd, 3rd, and 4th SBZ, which define the points X, S, and Y when they are reduced on the first BZ.

Figures 1b and c show LEED patterns, taken with 125.2 eV electrons for sample temperatures of 250 K (b) and 25 K (c), respectively. The left pattern reflects the single domain (4×1) reconstruction stable at high temperature whereas at 25 K the surface symmetry has changed to a (8 × 2) symmetry as revealed by the right pattern. Perpendicular to the chains, the new structure is commensurate as evidenced by the sharp 8× spot doubling in some regions. Along the chains, on the other hand,

the ×2-stripes indicate a small coherence length of the periodicity doubling. A simple model of a disordered structure has been shown to produce a LEED pattern quite similar to the one observed here. All chains have strictly the same double period but they have a random probability to be precisely in phase or out of phase with each other [23]. We note, though, that if the stripes were due to fluctuations, spots accounting for the commensurate low temperature ground state should appear below a certain crossover temperature T^* [5]. We emphasize that the stability of the diffraction pattern from the transition temperature down to 25 K seems to favor a disordered state rather than fluctuations. The fact that no highly ordered low temperature ground state appears down to 25 K does, however, not exclude its existence. Nonetheless, it is clear that the system undergoes a transition coupled to a lattice distortion on the surface.

To reveal changes in the electronic structure through the transition, we performed ARPES measurements as a function of temperature, for a fixed emission angle θ of 17°, corresponding to $0.74|\Gamma X| = \frac{\pi}{a} = 0.81\,\text{Å}^{-1}$, a being the surface lattice constant). The work function has been deduced from measurements of the high-energy ARPES cut-off to be 4.6±0.1 eV. Part (a) of Figure 2 displays raw data in a temperature range from 60 K up to 170 K. The arrows indicate the In-induced surface state bands (SSB) m_2 and m_3 according to Abukawa *et al.* [10]. The m_2 peak and the m_3 shoulder show a clear and abrupt shift of ~100 meV around 115 K. In order to evidence this, the inset (Fig. 2 part (b)) displays the energy position of the m_2 band as a function of temperature. The solid line serves as guide to the eye. These findings demonstrate the concomitance of the changes of the electronic and the crystal structure. The band dispersions and symmetries change as a function of temperature, which shall be presented in the next paragraph. We emphasize that this is not caused by surface photovoltage effects, which has not the sharp, transitory character of the shift observed here [24]. In addition, for the p-doped sample used here, a shift caused by surface photovoltage would be in the opposite direction.

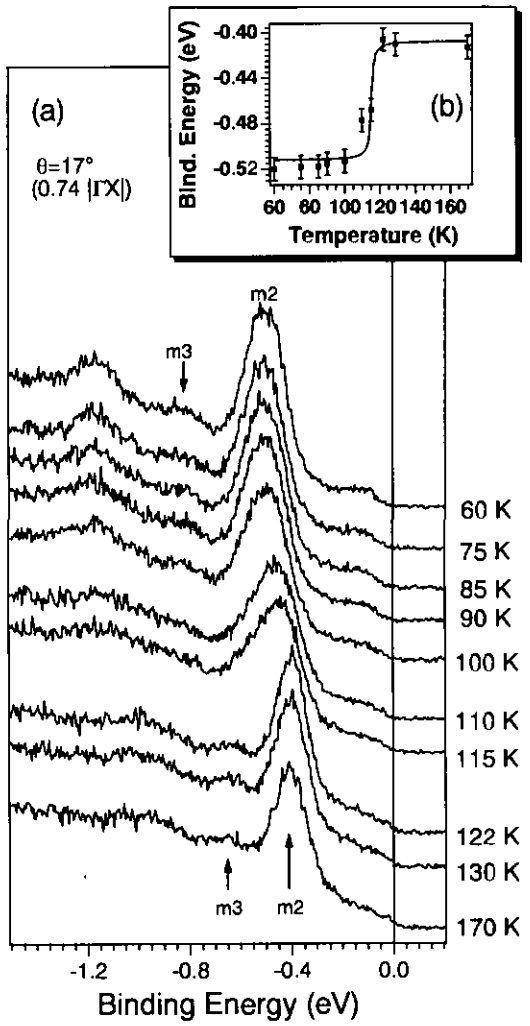

Fig. 2. (a) ARPES spectra of the Si(111)-(4 × 1)In surface taken at 17° emission angle for various temperatures around the transition at ~110 K. The inset (b) displays the peak energy of the surface state band m_2 as a function of temperature, the abrupt energy shift clearly indicating the transition. The solid line serves as guide to the eye.

We performed several cycles to pass the transition, its temperature T_c = 115 K remained constant within the accuracy of our measurement, but shows a slight hysteresis of the order of 10 K (not shown in Fig. 2 for simplicity). Our T_c value is slightly lower than that reported recently in an electron loss study [9].

Figure 3 shows ARPES spectra taken with p-polarised 21.2 eV photons as a function of the emission angle in the [1$\bar{1}$0]-direction or, in other words, along the In chains (ΓX in the SBZ, *cf.* Fig. 1 part (a)). The spectra, taken at 130 K are displayed in an angular range from 8° up to 27° off normal, or from $0.36|\Gamma X|$ to $1.17|\Gamma X|$. The X-point of the SBZ at 23° is indicated. One observes two crossings of the Fermi level E_F, for SSB m_2 at ~12° and for the SSB m_3 at ~10°, respectively, indicated by k_{F2} and k_{F3} in Figure 3. The m_2-SSB disperses downwards until a maximum binding energy of 400 meV at 18° before it broadens and seemingly splits off into two peaks, one of them remaining almost dispersionless, the other, however, moving backwards towards E_F. The m_3-SSB is visible as faint shoulder with slightly higher binding energy than m_2 (200 meV shift with respect to m_2). The other dominant structure seen at ~1.0 eV in the 8° spectrum consists of two contributions which are consistent with a previous study [10].

Figure 4 presents ARPES spectra taken in the same angular range as in Figure 3, but now at 60 K. Several essential new features are evident. Firstly, the m_2-SSB shows a distinct shift, as already observed in Figure 2. Secondly, even more important, the backdispersing feature seen at emission angles from 21° to 24° in the high temperature data (*cf.* Fig. 3) has completely disappeared. Thirdly, Fermi level crossings are no longer visible indicating that the system has undergone a metal-insulator transition.

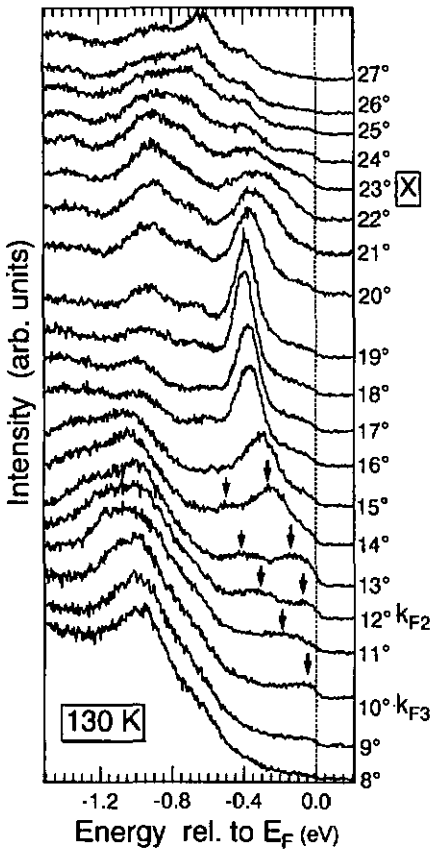

Fig. 3. ARPES data along the chain direction, taken at 130 K with linearly polarised 21.2 eV photons. The emission angle and the X-point of the surface Brillouin zone (SBZ) are indicated. The arrows denote the Fermi level crossings of the two main bands of interest, the m_2 and the m_3 surface state bands.

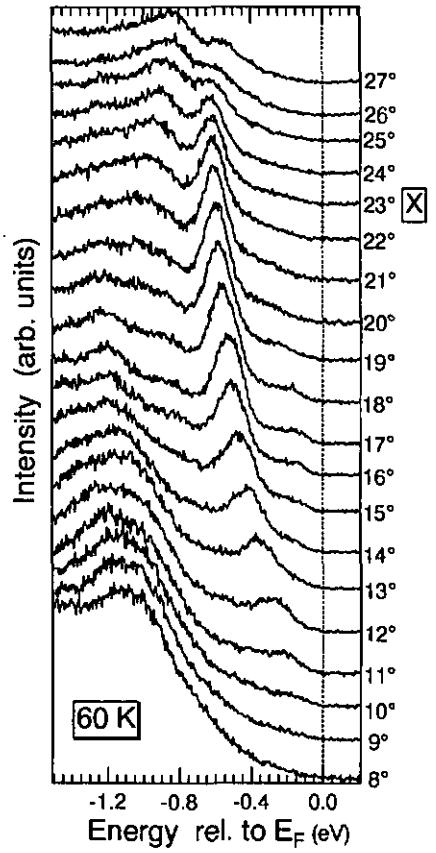

Fig. 4. ARPES data along the chain direction, now taken at 60 K with linearly polarised 21.2 eV photons. The emission angle and the X-point of the surface Brillouin zone (SBZ) are indicated.

In order to better visualize spectral changes as a function of temperature, we map in Figure 5 the dispersion of the essential features from Figures 3 and 4. Energy positions have been precisely obtained by subtracting a Shirley background and fitting the corrected curves to Lorentzian lines multiplied with a Fermi-Dirac distribution. As we are interested in the shape of the dispersion curves rather than in the precise lineshape and/or in lifetimes, this procedure is very suitable to deduce the band structure. The top and bottom panel show the results for the 130 K and 60 K data, respectively. The circles and triangles give the dispersion for the m_2 and m_3 SSB, respectively. Squares show faint structures on the spectra (*cf.* Fig. 4), which can not be assigned to clear spectral features. The two black bars indicate the sudden increase in peak width around the S-point as seen in the spectra in Figure 3. There are several important observations to be addressed. The m_2 SSB is shifted considerably upon cooling (*cf.* Figs. 3 and 4), and the m_3 SSB is barely detectable at 60 K, being only present as a very faint shoulder in some spectra of Figure 4. Most importantly, all dispersive features which seem at first sight to simply follow the extremum condition imposed by the border of the BZ at $X = 0.81$ Å^{-1} have a more complex behavior. At 130 K, the apparent splitting of the SSB m_2 mentioned previously occurs rather at 0.75 Å^{-1} than at the expected value of 0.81 Å^{-1} and in the dispersion of both bands, the gradient seems to change near 0.55 Å^{-1} and 0.75 Å^{-1}. These anomalous features cannot be explained for states belonging to the first SBZ. Therefore, we have reported as dashed lines in Figure 5 (top) the points S and Y from the (4 × 1) reduced zones, as defined in Figure 1. The k-values for these points are $S = |\Gamma X| \times \frac{11}{12} = 0.75$ Å^{-1} and $Y = |\Gamma X| \times \frac{2}{3} = 0.54$ Å^{-1}. The band structure observed here has not been resolved in such detail in former work [8,10], probably due to moderate energy resolution and we point out that in particular the backdispersing feature around S and X has not been found elsewhere.

As can be observed in the ARPES spectra presented in Figures 3 and 4, both the m_2 and the m_3 SSB show a clear crossing of the Fermi level at 130 K. The exact value of the two Fermi vectors ($k_{F2} = 0.43 \pm 0.04$ Å^{-1} and $k_{F3} = 0.34 \pm 0.04$ Å^{-1}) are obtained by extrapolating the dispersion curves at 130 K (Fig. 5). In order to better characterize the transition, high-resolution spectra have been performed at precisely these two k-values

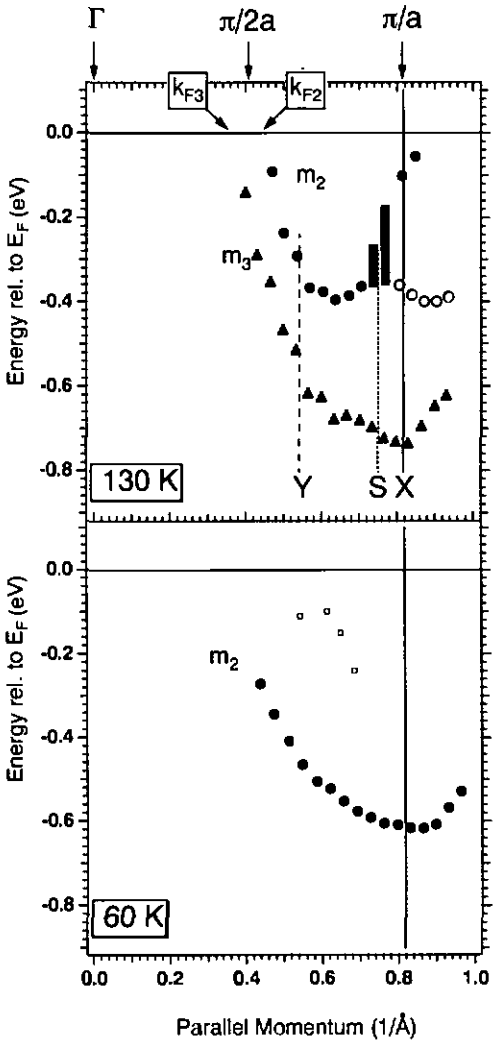

Fig. 5. Dispersion curves for the main bands derived from the ARPES spectra in Figure 3 (top panel) and Figure 4 (bottom panel). Details of the analysis are found in the text. The SBZ boundary corresponding to the Si(111)-(4 × 1)-In symmetry is given by the black line at 0.81 Å^{-1}. The singular points S and Y stem from higher order SBZs (see text). The Fermi vectors $\mathbf{k}_{F2}$ and $\mathbf{k}_{F3}$ are indicated. For the sake of clarity we display on top the positions for Γ, π/a, and $\pi/2a$. The latter value corresponds to half of the nesting vector for perfect nesting.

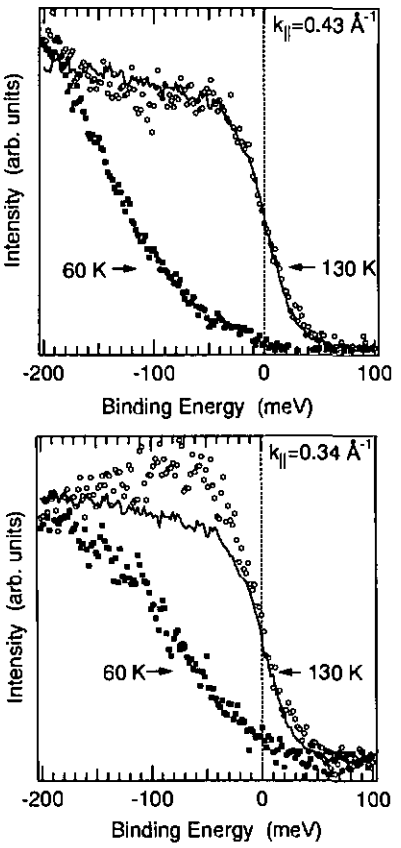

Fig. 6. ARPES spectra of the m_2 band (top) and the m_3 band (bottom) for 130 K (open symbols) and 60 K (filled symbols) at the high-temperature Fermi vectors $\mathbf{k}_{F2}$ and $\mathbf{k}_{F3}$. Superimposed on the spectra are data obtained from the molybdenum sampleholder taken at 130 K (solid lines).

above and below the transition. The results are displayed in Figure 6. The top and bottom panel show the spectra for $k_{||} = 0.43$ Å^{-1} and $k_{||} = 0.34$ Å^{-1}, respectively, and in both panels, open and filled symbols denote spectra taken at 130 K and 60 K, respectively. The solid lines are spectra taken on the molybdenum sampleholder at 130 K in order to compare the high temperature data to the Fermi level of a conventional metal. One clearly observes a Fermi step above the transition, whereas below the transition, both spectra exhibit clear leading edge shifts. We point out, that the transition is apparent in *both* bands, although in both cases weak Fermi steps remain visible meaning that the gapping is incomplete. An exact gap value is hard to find because both bands reveal a rigid shift below T_c where wave vectors corresponding to the Fermi vectors above T_c can only be given approximately. In contrast to the present observation only a single band has been previously assumed to be involved in the transition [8].

4 Discussion

Despite the clear structural information on the high-temperature (4 × 1)-phase delivered by the LEED data (Fig. 1), the band dispersions extracted from the corresponding photoemission spectra exhibit unusual and complex shapes impeding a straightforward deduction of the surface electronic states. In the region measured in our experiment, *i.e.*, from Γ to X, only two of the 3 known bands [10] are clearly observed, namely m_2 and m_3(*cf.* Fig. 3). The most surprising aspect of the dispersion of these two bands is their uncertain and diffuse behavior around the point X of the first SBZ border (Fig. 5). When the higher order SBZs shown in an extended zone

scheme in Figure 1a are reduced to the first SBZ, new zone borders cross the axis ΓX and define singular points which may have to be taken into consideration, namely the S- and the Y-point from the 2nd SBZ and the 4th SBZ, respectively. In Figure 3, the m_2 SSB shows a broadening close to the S-point followed by the emergence of an upward dispersing band which may result from a splitting.

We may speculate that the SBZ border at S is the origin of this peculiar observation but in such a case, one would expect to observe a gap and a backfolded band induced by the new symmetry. The magnitude of the involved gap resulting from the scattering at crystalline planes containing a low density of lattice points is probably too small to be observed, if one accounts for inherent lifetime broadening and resolution effects. The main consequence in the spectra should be a width increase, a fact that we actually observe (see Fig. 5, where the black bars denote the peak width increase). Backfolding of bands symmetrically to BZ boundaries is not unambiguously observed in Figure 3, and the origin of the separation of the m_2 state in one branch moving towards E_F, the other one keeping a rather flat dispersion, remains uncertain. Such a situation is possibly explained by a recent model calculation [25] showing that the photoemission intensity keeps mainly concentrated on wave vector values given in the extended zone scheme. When a band represented in the extended zone scheme is followed across a zone boundary, its intensity falls off rapidly in the neighbor repeated zone. The importance of this mechanism is confirmed by the differences between ARPES spectra recorded along Γ_1X_1 and Γ_3X_3 as observed earlier [8,10]. In the present study, it contributes certainly to the unconventional dispersions of the m_2 and m_3 states and one cannot exclude that the peak approaching E_F above X accounts for a small portion of the m_1 band previously identified in this range [10]. A detailed interpretation of our data in the complicated **k**-space region around the point X is hazardous without a reliable band structure calculation requiring a confirmed crystalline structure.

In the low temperature phase, the periodicity change from 4× to 8× perpendicular to the chains results in a denser distribution of the border lines of the higher order BZs. This increased complexity is not reflected by the dispersion of the m_2 state clearly observed at 60 K (Fig. 4). Apart from a rigid shift of approximately 100 meV, the overall shape of its dispersion is not markedly modified. However, the step-like irregularities observed above T_c are replaced by a smooth behavior and the splitting of m_2 has completely disappeared. Maybe the high density of zone boundaries with the gapping and weak backfolding of the bands crossing are no longer detectable in ARPES. On the other hand, a careful inspection of Figure 4 shows that m_2 seems to continue to disperse towards smaller wave vectors than its Fermi vectors $\mathbf{k}_{F2}$ in the high-temperature phase. Therefore, it is not obvious that the population of the bands remains constant through the transition as in a conventional Peierls system. The shift of the states below the transition is likely to increase the population of the m_2 and m_3 bands. If the number of available electrons remains constant, maybe m_1 which is no longer observed, is depopulated by this mechanism below T_c.

We turn now to the discussion of the mechanism driving the phase transition which must be closely related to periodicity doubling in the chain direction. In a one-dimensional system with a single metallic band, the Peierls transition is accomplished by the formation of a CDW with a fixed nesting vector $\mathbf{q} = 2\mathbf{k}_F$, together with a static distortion of the lattice leaving the system below the transition in an insulating ground state with a commensurate CDW and the opening of the Peierls gap Δ at $\mathbf{k}_F$ [5]. In the present case, a single nesting vector cannot be responsible for the simultaneous opening of a gap in 2 bands near their high temperature Fermi vectors $\mathbf{k}_{F2}$ and $\mathbf{k}_{F3}$, as shown in Figure 6. A flat dispersion near $\mathbf{k}_F$ revealing a gap opening is not observed either and even a weak intensity at E_F persists in this range (see Fig. 6). These facts are qualitatively consistent with the disordered or fluctuating ×2 symmetry suggested by the stripes in LEED (Fig. 1). A sharp and commensurate nesting vector would have the value $q = 0.81$ Å^{-1} which is intermediate between $2k_{F3} = 0.68$ Å^{-1} and $2k_{F2} = 0.86$ Å^{-1}. It has been a matter of debate [26–28], what happens in a quasi-1D system, when there are competing bands crossing E_F. $NbSe_3$ is one example [29], where successive transitions occur related to the formation of different CDWs. Down to 25 K, however, only one transition occurs in the present case, making this model very unlikely. Another possibility is encountered in blue bronze $K_{0.3}MoO_3$, where recent studies [28] revealed that the existence of two Fermi wave vectors can result in the formation of a single CDW, however with a temperature dependent wave vector. Calculations of Noguera [27] show that for two 1D bands crossing the Fermi level at different wave vectors, there is the possibility of a second-order Peierls transition with the opening of a small gap on each band. The data available up to now on the Si(111)-(4 × 1)-In system are not incompatible with this type of prediction but it is very delicate to deduce a final picture. Obviously, the phase transition is mediated by a symmetry modification related to the Fermi wave vectors resulting in an overall energy lowering of the electronic states. It is interesting to notice that the low-temperature phase, in contrast to the fluctuation theory of Lee *et al.* [30], has less order than the high-temperature phase. The difference here is that disorder stabilizes the low-temperature phase and is not a high-temperature precursor state.

In summary, we presented ARPES measurements as a function of temperature for the quasi-1D chain system Si(111)-(4 × 1)-In. From our LEED data we established that the transition from a high temperature (4 × 1)- to a low temperature (8 × 2)-phase is reversible and sharp with a small hysteresis of the order 10 K around 115 K. ARPES spectra reveal clearly important concomitant changes in the electronic band structure near the Fermi surfaces and at the border of the BZ. We derived the detailed dispersive behavior of the bands involved in the transition and could demonstrate that at least the two surface state bands m_2 and m_3 show the opening of a pseudo energy gap on the Fermi surface leaving small but finite spectral weight in

the low-temperature state. We conclude that this transition is probably driven by a similar but more complex mechanism than in a conventional Peierls transition.

We gratefully acknowledge fruitful discussions with I. Matsuda. This work was supported by the Fonds National Suisse de la Recherche Scientifique.

References

1. M. Grioni J. Voit, *in Electron Spectroscopies Applied to Low-Dimensional Materials*, edited by H.P. Hughes, H.I. Starnberg (Kluwer Academic Publishers, 2000) p. 209.
2. J.M. Luttinger, J. Math. Phys **4**, 1154 (1963).
3. P. Segovia, D. Purdie, M. Hengsberger, Y. Baer, Nature (London) **402**, 504 (1999).
4. R.F. Peierls, *Quantum Theory of Solids* (Clarendon Press, Oxford, 1955) p.108.
5. G. Grüner, *Density Waves in Solids* (Addison-Wesley, Reading (MA), 1994).
6. B. Dardel, D. Malterre, M. Grioni, P. Weibel, Y. Baer, F. Lévy, Phys. Rev. Lett. **67**, 3144 (1991).
7. B. Dardel, D. Malterre, M. Grioni, P. Weibel, Y. Baer, C. Schlenker, Y. Pétroff, Europhys. Lett. **19**, 525 (1992).
8. H.W. Yeom, S. Takeda, E. Rotenberg, I. Matsuda, K. Horikoshi, J. Schaefer, C.M. Lee, S.D. Kevan, T. Ohta, T. Nagao, S. Hasegawa, Phys. Rev. Lett. **82**, 4898 (1999).
9. K. Sakamoto, H. Ashima, H.W. Yeom, W. Uchida, Phys. Rev. B **62**, 9923 (2000).
10. T. Abukawa, M. Sasaki, F. Hisamatsu, T. Goto, T. Kinoshita, A. Kakizaki, S. Kono, Surf. Sci. **325**, 33 (1995).
11. M.K. Kelly, G. Margaritondo, J. Anderson, D.J. Frankel, G.J. Lapeyre, J. Vac. Sci. Technol. A **4**, 1396 (1986).
12. M. Kawaji, S. Baba, A. Kinbara, Appl. Phys. Lett. **34**, 748 (1979).
13. J. Kraft, G. Ramsey, F.P. Netzer, Phys. Rev. B **55**, 5384 (1997).
14. I.G. Hill, A.B. McLean, Phys. Rev. B **56**, 15725 (1997).
15. J. Nogami, S. Park, C.F. Quate, Phys. Rev. B **36**, 6221 (1987).
16. H. Öfner, S.L. Surnev, Y. Shapira, F.P. Netzer, Phys. Rev. B **48**, 10940 (1993).
17. I.G. Hill, A.B. McLean, Phys. Rev. B **59**, 9791 (1999).
18. J.L. Stevens, M.S. Worthington, I.S.T. Tsong, Phys. Rev. B **47**, 1453 (1993).
19. N. Nakamura, K. Anno, S. Kono, Surf. Sci. **256**, 129 (1991).
20. A.V. Zotov, A.A. Saranin, O. Kubo, T. Harada, M. Katayama, K. Oura, Appl. Surf. Sci. **159-160**, 237 (2000).
21. O. Bunk, G. Falkenberg, J.H. Zeysing, L. Lottermoser, R.L. Johnson, M. Nielsen, F. Berg-Rasmussen, J. Baker, R. Feidenhans'l, Phys. Rev. B **59**, 12228 (1999).
22. C. Kumpf, O. Bunk, J.H. Zeysing, Y. Su, M. Nielsen, R.L. Johnson, R. Feidenhans'l, K. Bechgaard, Phys. Rev. Lett. **85**, 4916 (2000).
23. H. Lipson, K.E. Singer, J. Phys C. **7**, 12 (1974).
24. J.E. Demuth, W.J. Thompson, N.J. DiNardo, R. Imbihl, Phys. Rev. Lett. **56**, 1408 (1986).
25. J. Voit, L. Perfetti, F. Zwick, H. Berger, G. Margaritondo, G. Grüner, H. Höchst, M. Grioni, Science **209**, 501 (2000).
26. C. Noguera, J.-P. Pouget, J. Phys. I France **1**, 1035 (1991).
27. C. Noguera, J. Phys. C. **19**, 2161 (1986).
28. A.V. Fedorov, S.A. Brazovskii, V.N. Muthukumar, P. Johnson, J. Xue, L.-C. Duda, K.E. Smith, W.H. McGarroll, M. Greenblatt, S.L. Hulbert, J. Phys. Cond. Matt. **12**, L191 (2000).
29. P. Monceau, *Electronic Properties of Inorganic Quasi-One-Dimensional Compounds* (Dordrecht: Reidel, 1985).
30. P.A. Lee, T.M. Rice, P.W. Anderson, Phys. Rev. Lett. **31**, 462 (1973).

Publication [2]

O. Gallus, Th. Pillo, P. Starowicz, and Y. Baer, *Honeycomb chain-channel (HCC) signature in the calcium-induced Si(111)-(3×2) surface*, Europhysics Letters **60**, 903 (2002).

EUROPHYSICS LETTERS 15 December 2002

Europhys. Lett., **60** (6), pp. 903–909 (2002)

Honeycomb chain-channel (HCC) signature in the calcium-induced Si(111)-(3 × 2) surface

O. GALLUS, TH. PILLO, P. STAROWICZ and Y. BAER

Institut de Physique, Université de Neuchâtel
Rue A.-L. Breguet 1, CH-2000 Neuchâtel, Switzerland

(received 8 July 2002; accepted in final form 2 October 2002)

PACS. 73.20.At – Surface states, band structure, electron density of states.
PACS. 79.60.-i – Photoemission and photoelectron spectra.
PACS. 68.35.-p – Solid surfaces and solid-solid interfaces: Structure and energetics.

Abstract. – The electronic and structural properties of a calcium-induced chain system on Si(111) have been studied. Low-energy electron diffraction measurements clearly reveal a (3 × 2) periodicity and the Ca coverage is determined to be 1/6 monolayer. Angle-resolved photoemission measurements bave been performed with two different light polarizations in order to study tbe symmetries of the surface states. In both polarizations no band crossing the Fermi level E_F is found. The three detected surface state bands are in good agreement with theoretical calculations in the honeycomb chain-channel (HCC) model for an insulating case.

Introduction. – In the past decade quasi–one-dimensional (1D) systems gained a great interest and have been the subject of various studies. Highly anisotropic crystals have offered quite interesting possibilities to investigate the properties resulting from a low dimensionality. Another approach consists in the preparation of 1D self-ordering surface structures obtained by evaporating an adsorbate submonolayer on a single-crystal surface followed by annealing. The use of an insulating substrate favours the creation of surface electronic structures that are only weakly coupled to the bulk. Among this type of surfaces, some popular systems were investigated, *i.e.* the Si(111)-(4 × 1)In surface containing chains exhibiting a Peierls-like phase transition [1, 2]. Angle-resolved photoemission (ARPES) spectra [3] of Si(557)-(5 × 1)Au showed a non–Fermi-liquid behavior, revealing the 1D metallic character of this system, although the exact nature of this surface remains controversial [4, 5]. Another interesting family of surface structures are the (n × 1) reconstructions induced on Si(111) by deposition of monovalent alkali metals (AMs) and divalent alkali earth metals (AEMs). For example, Ca stabilizes reconstructions for n = 7, 5, 3 and 2 [6, 7]. This kind of surfaces were examined in various studies and several structures including the so-called honeycomb chain channels (HCC) [6–12], as well as other models [6, 7, 12–24] were proposed and discussed in the light of experimental results. Recently, the (3 × 1) surfaces have gained a particular interest and the results of numerous studies using different measurement techniques lead to the conclusion that the surface structures induced by AMs [8, 9, 12, 13, 16, 19, 21] as well as by AEMs [6, 7, 10–12, 23–25] are likely to be very similar. Among the proposed structures, a

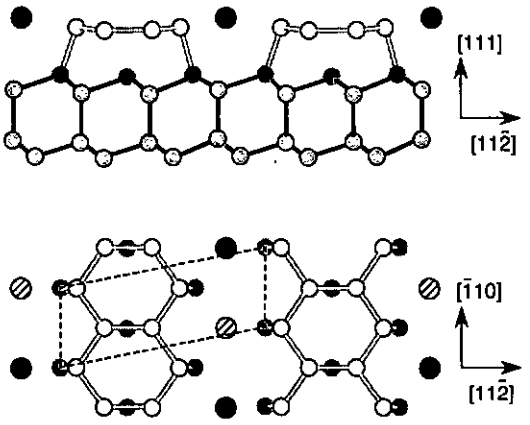

Fig. 1

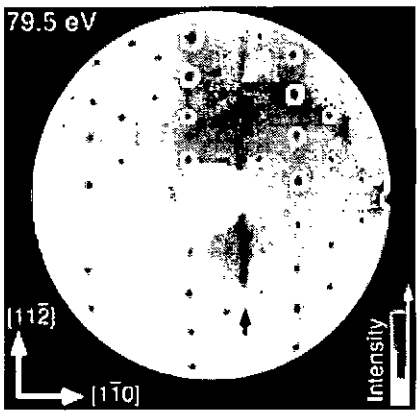

Fig. 2

Fig. 1 – The honeycomb chain channel structure. The adsorbate atom positions are shown by the hatched and full black circles. They are located between the HCC channels formed by silicon atoms. The dashed parallelogram shows the (3×1) unit cell for the Si-HCC. The situation where all adsorbate atom positions are occupied corresponds to a coverage of 1/3 monolayer. For a calcium coverage of 1/6 monolayer only half of the positions must be occupied (either the hatched or the full circles). In the latter case, one obtains a double periodicity along the calcium chains with respect to the HCC channels.

Fig. 2 – Grey-scale inverted LEED pattern of the preferential single domain Si(111)-(3×2)Ca surface obtained for an electron energy of 79.5 eV. The black arrow shows a faint stripe indicating a $2a$ periodicity along the chains.

recent study [8] showed the HCC model to be energetically the most favorable. In this model, the surface consists of adsorbate atoms forming linear chains located in the channels of the HCC structure formed by the Si atoms as shown in fig. 1. A straightforward prediction about the electronic structure of the two types of (3×1) surfaces with AM and AEM adsorbates raises a confusing situation. In fact, the Si(111)-(3×1)AM surfaces with 1/3 monolayer (ML) of monovalent atoms are insulating as verified in several ARPES studies for Na [15], Li [17] and K [18]. Therefore, with a coverage that was supposed to be the same for the divalent AEM-induced (3×1) reconstruction, a simple one-electron description of the same surface structure leads to the conclusion that this surface should be metallic as a consequence of the additional valence electron. However, recent studies of the (3×1) reconstruction stabilized with Mg [22] and Ca [6] showed an insulating character of the surface states induced by these AEMs. Different models have been suggested in order to explain this unexpected insulating character of the AEM (3×1) systems. One proposition was that these surfaces could be of the Mott insulator type [22]. In a theoretical work about the HCC model, Erwin and Weitering [8] attempt to explain the non-observation of any peak crossing the Fermi level as the consequence of a peculiar aspect of the photoemission process in the Mg(3×1) surface [22]. They argue that the photoemission matrix elements for surface states having particular symmetries can become vanishingly small in certain experimental configurations using polarized photons. Finally, it was also suggested that this surfaces could exhibit a Peierls instability with the formation of a charge density wave (CDW) [6]. This assumption is supported by the fact that a $2a$ periodicity (a being the surface lattice constant) in the chains direction showed up in various experimental studies [6,7,24,25]. It is important to note that in a recent STM work on the Ba-induced HCC structure, Lee *et al.* [10] showed that this surface has a

(3×2) periodicity and stabilizes with 1/6 ML of Ba atoms. The insulating character they observe by tunneling spectroscopy is explained without involving strong correlation effects. In the present paper, we report the results of our experiments of the Si(111)-(3×2)Ca surface. We performed ARPES and low-energy electron diffraction (LEED) measurements, as well as coverage determinations, using Auger electron spectroscopy (AES) and a quartz crystal microbalance (QCM). The photoemission spectra were recorded with two different light polarizations in order to ensure that all bands can be detected. The surface is found to be insulating for a Ca coverage of 1/6 ML. The characteristics of the system are discussed and the three surface state bands observed in the spectra are compared to the HCC predictions.

Experiment. – The calcium-induced reconstruction was produced using p-doped ($\rho \sim 5\,\Omega\,\mathrm{cm}$) vicinal Si(111) wafers having a miscut of 1.1° towards the $[\bar{1}\bar{1}2]$-direction allowing predominantly single domain growth. The samples ($5 \times 19 \times 0.5\,\mathrm{mm}^3$) were heated using direct current in the direction of the channels. Ca was evaporated from a water-cooled Knudsen cell-type evaporator at pressures better than 5×10^{-10} mbar. The quantities were calibrated with a QCM and confirmed by X-ray photoelectron spectroscopy (XPS) and AES used to control the composition and cleanness of the surface. After the evaporation of Ca on the clean Si(111)-(7×7) surface held at room temperature (RT), the sample was annealed to 600 °C where the surface reconstruction formed. The symmetry and quality of the ordered structure were observed with LEED. ARPES measurements were performed using a SCIENTA SES-200 electron spectrometer with a hemispherical electron analyzer and a two-dimensional detector. The spectra were excited with s- and p-polarized photons (corresponding to polarization perpendicular and in the measurement plane, respectively) with an energy of 21.2 eV. The energy and angular resolution were, respectively, 5 meV and ±0.5°.

Results and discussion. – Figure 2 shows the LEED pattern of our Si(111)-(3×2)Ca surface with one dominant orientation and insignificant contributions from the two others. A careful inspection of this image reveals faint stripes indicating a $2a$ periodicity in the direction of the chains. Similar stripes were reported in former studies of surfaces with different AEM, using reflection high-energy electron diffraction (RHEED) [6, 7], and LEED [11, 24, 25]. In studies [6, 22] where the Ca and Mg coverage inducing the reconstruction was assumed to correspond to 1/3 ML, the simplest approach was predicting metallic bands. The unexpected observation of insulating bands was associated to the $2a$ periodicity supposed to reflect the formation of charge density waves [6]. However, beside this electronic interpretation of the periodicity doubling, one has also to consider models based on the structure. Such approaches are supported by recent studies of surface reconstructions with Ca [7], Mg [24] and Ba [10], where the surface symmetry is proposed to be a combination of (3×2) and $c(6 \times 2)$, suggesting that these symmetries reflect the adsorbate structure. In this situation, it is useful to carefully investigate the crystallographic and electronic structure resulting from Ca adsorption. In this respect, it is important to re-examine the precise Ca coverage corresponding to the (3×2) LEED pattern. The obtained information is essential to make a realistic prediction of a structure compatible with the insulating character of this surface.

We have measured, with our QCM, a Ca quantity on the (3×2) surface corresponding to a coverage close to 1/6 ML (the atom density of the bulk-terminated Si(111) surface of $7.8 \times 10^{14}\,\mathrm{cm}^{-2}$ was used as standard for 1 ML). However, as such quantitative measurements are affected by quite large uncertainties (limited sensitivities, sticking coefficients, specific experimental configuration...), we have performed with AES another independent determination of this coverage by comparing the AES intensities of Ag in Si(111)-(3×1)Ag [26] to those obtained for Ca in Ca(3×2). By taking the widely accepted coverage of 1/3 ML for the Ag(3×1) surface [27], and using the relative AES sensitivities between Ag and Ca, the

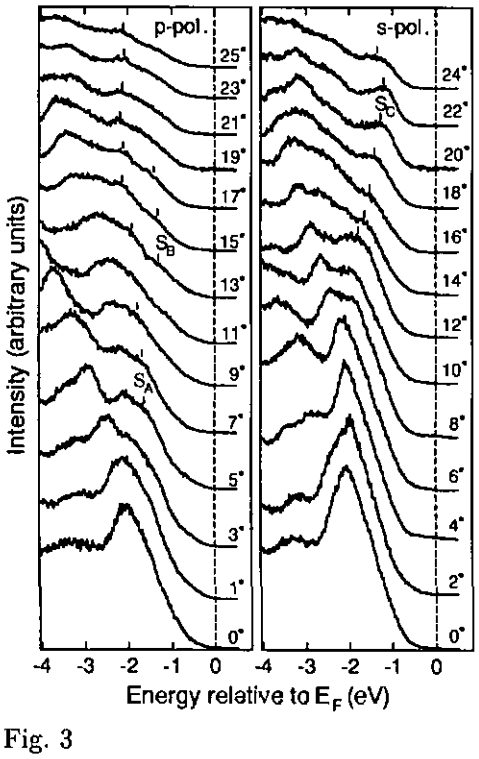

Fig. 3

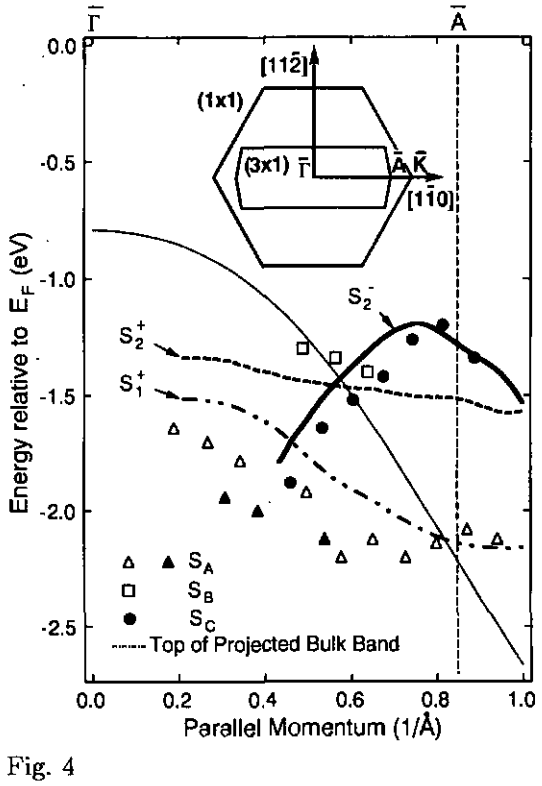

Fig. 4

Fig. 3 – Angle-resolved photoemission spectra of the Si(111)-(3 × 2)Ca surface. Spectra were taken at room temperature along the [1$\bar{1}$0] direction (*i.e.* along the chains), using *p*- and *s*-polarized photons of 21.2 eV energy. Three surface state bands are labelled by S_A, S_B and S_C.

Fig. 4 – Dispersion of the three measured surface bands S_A, S_B and S_C along the $\bar{\Gamma}\bar{A}$ direction of the (3 × 1) surface Brillouin zone (see the inset). Open and solid symbols indicate the position of the peaks measured with *p*- and *s*-polarization, respectively. The lines labelled by S_1^+, S_2^+ and S_2^- were obtained from fig. 2 of ref. [8]. They were rigidly shifted by 0.9 eV with respect to their energy position in ref. [8].

QCM results were confirmed and the conjunction of both techniques leads to a Ca coverage of 1/6 ML with an accuracy of 30%.

We now turn to our ARPES measurements of the Ca(3 × 2) surface. Figure 3 shows the spectra obtained with 21.2 eV photons, for wave vectors along the $\bar{\Gamma}\bar{A}$ direction of the surface Brillouin zone (SBZ) (see the inset of fig. 4). The spectra were obtained using *p*- as well as *s*-polarisation. Three non-metallic Ca-induced surface state bands, labelled by S_A, S_B and S_C, were observed. A small contribution to the spectral weight close to the Fermi level, stemming from a few remaining (7 × 7) regions of pure silicon, could not completely be avoided. Therefore, we conclude that the Ca(3 × 2) reconstruction is insulating with a gap close to 1 eV. In the spectra obtained with the two different polarizations one remarks strong differences in the peak ratios. For example, the band S_C is easily observed at emission angles around 20° with *s*-polarization but it is not detected with *p*-polarization. The dispersive behaviour of the three surface state bands (fig. 3) are given in fig. 4. The three lines labelled by S_1^+, S_2^+ and S_2^- have been taken from fig. 2 of ref. [8] and reproduced in our fig. 3 with a shift of 0.9 eV. They account for the calculated band structure of Li(3 × 1) within the HCC model and we attempt to compare them to our bands S_A, S_B, and S_C measured for Ca(3 × 2). Our band S_C

has a hole-like dispersion that matches very well the theoretical behavior of band S_2^-. This band is predicted to be only observable in the *s*-polarized configuration of our experiment. This is exactly the case for band S_C and therefore we associate S_C to S_2^-. Bands S_A and S_B are crossing S_C at two distinct wave vector positions, in good agreement with the crossing of bands S_1^+ and S_2^+ with band S_2^-. Consequently, we associate S_A and S_B to S_1^+ and S_2^+, respectively. This good accordance between our three measured surface states and the band structure calculation suggests that the description of the Si(111)-(3 × 2)Ca surface can be given on the basis of the HCC model of Si(111)-(3 × 1)Li. In fact, Erwin and Weitering have done their HCC calculation for a surface with 1/3 ML of adsorbed Li atoms. The structure corresponding to this situation is illustrated in fig. 1. One has just to occupy all indicated adsorbate atom positions (hatched and full black circles) with Li atoms. In this situation with one monovalent Li atom per (3 × 1) unit cell, a simple electron count leads to an even number (6) of electrons (5 stemming from Si and one from Li [8]) filling the three surface bands S_1^+, S_2^+, and S_2^- (fig. 4), in agreement with the observed insulating character of this surface [17]. If one considers now that Li atoms are just replaced by Ca atoms (1/3 ML of Ca), the additional valence electron would lead to a half-filled metallic state.

However, we measured a Ca coverage of 1/6 ML and one has to assume that only half of the adsorbate atom positions (fig. 1) are occupied. Consequently, the calcium chains have a $2a$ periodicity but they can occupy two different positions (hatched or filled circles). Adjacent chains can be in phase or out of phase and it has been simulated [28] and verified for other surfaces [2] that a stochastic distribution of these relative positions produces "×2" stripes at half distance between the (3 × 1) LEED spots. Our observation of such a pattern (fig. 2) provides a further confirmation of the 1/6 ML calcium coverage. It results that for calcium, 2 electrons per (3 × 2) unit cell are donated by the adsorbate and this situation shows striking similarities with the (3 × 1) reconstruction induced by AMs with 1 donated electron per unit cell. Also *it* is in agreement with the proposal of Lee *et al.* [10] that the HCC structure is stabilized by one donated electron per (3 × 1) cell of the silicon atoms. The most obvious consequence is that in both cases the surface bands induced by the adsorbates have an insulating character. In first approximation, one can anticipate that the (3 × 2)Ca bands can be obtained from a simple backfolding of the (3 × 1)Li bands if the new gaps are sufficiently small. Then, the successful comparison of the dispersions of the two reconstructions results from the fact that the photoemission structures are predominantly observed in the extended zone scheme [29]. The validity of an interpretation of the electronic structure of the (3 × 2)Ca surface on the basis of the calculated (3 × 1)Li surface, which was recently given in a similar way for the barium-induced case [11], implies that the HCC structure of the Si atoms forms a stable framework. This assumption is supported by a series of works. STM and mass transport measurements of the AEMs Ca and Mg, as well as of the AMs Li and Na have all [12, 13, 16, 24, 25] concluded that the Si top layer density of such reconstruction is 4/3 ML, consistent with the HCC model. The LEED *I-V* curves for the Li, Na and Mg induced reconstructions were found to be very similar [19, 23]. This lack of dependence on the different adsorbates indicates that the diffraction is essentially determined by the Si surface atoms forming the same reconstruction.

Conclusion. – We have shown that a coverage of 1/6 ML of Ca on Si(111) induces a (3 × 2) reconstruction corresponding to chains of AEM atoms with double periodicity and a random distribution of their two relative positions. The silicon atoms form a stable framework described by the HCC model and the Ca atoms are adsorbed in the channels. The insulating character of this structure is quite naturally explained by a simple electron count as in the case of the (3 × 1) reconstruction induced by the AM. We can discard earlier suggestions of CDW,

Peierls transition or Mott insulator concepts invoked in order to explain the insulating nature of this surface. It is interesting to notice that an insulating character has also been observed for the other reconstructions (7×1), (5×1) and (2×1) stabilized on Si(111) by different Ca concentrations [6]. These results indicate that in reconstructions induced by adsorbate sub-monolayers on insulating substrates, the electronic energy lowering resulting from a gap formation plays a dominant role in the stabilisation of the structure.

Additional Remark. Simultaneously with the submission of our manuscript, a study of the Si(111)-(3×1)Ca surface has been published [30]. It suggests structural and electronic properties similar to those derived from the present measurements.

* * *

We thank M. BOVET and P. AEBI for band structure calculations. This work was supported by the Fonds National Suisse de la Recherche Scientifique.

REFERENCES

[1] YEOM H. W., TAKEDA S., ROTENBERG E., MATSUDA I., HIROKOSHI K., SCHÄFER J., LEE C. M., KEVAN S. D., OHTA T., NAGAO T. and HASEGAWA S., *Phys. Rev. Lett.*, **82** (1999) 4898.
[2] GALLUS O., PILLO TH., HENGSBERGER M., SEGOVIA P. and BAER Y., *Eur. Phys. J. B*, **20** (2001) 313.
[3] SEGOVIA P., PURDIE D., HENGSBERGER M. and BAER Y., *Nature (London)*, **402** (1999) 504.
[4] LOSIO R., ALTMANN K. N., KIRAKOSIAN A., LIN J. L., PETROVYKH D. Y. and HIMPSEL F. J., *Phys. Rev. Lett.*, **86** (2001) 4632.
[5] ROBINSON I. K., BENNET P. A. and HIMPSEL F. J., *Phys. Rev. Lett.*, **88** (2002) 6104.
[6] BASKI A. A., ERWIN S. C., TURNER M. S., JONES K. M., DICKINSON J. W. and CARLISLE J. A., *Surf. Sci.*, **476** (2001) 22.
[7] SEKIGUCHI T., SHIMOKOSHI F., NAGAO T. and HASEGAWA S., *Surf. Sci.*, **493** (2001) 148.
[8] ERWIN S. C. and WEITERING H. H., *Phys. Rev. Lett.*, **81** (1998) 2296.
[9] KANG M. H., KANG J. H. and JEONG S., *Phys. Rev. B.*, **58** (1998) R13359.
[10] LEE G., HONG S., KIM H., SHIN D., KOO J. Y., LEE H. I. and MOON D. W., *Phys. Rev. Lett.*, **87** (2001) 056104.
[11] OKUDA T., ASHIMA H., TAKEDA H., AN K. S., HARASAWA A. and KINOSHITA T., *Phys. Rev. B*, **64** (2001) 165312.
[12] SARANIN A. A., ZOTOV A. V., LIFSHITS V. G., KATAYAMA M. and OURA K., *Surf. Sci.*, **426** (1999) 298.
[13] SARANIN A. A., ZOTOV A. V., LIFSHITS V. G., RYU J.-T., KUBO O., TANI H., HARADA T., KATAYAMA M. and OURA K., *Phys. Rev. B*, **58** (1998) 3545.
[14] JEON D., HASHIZUME T., SAKURAI T. and WILLIS R. F., *Phys. Rev. Lett.*, **69** (1992) 1419.
[15] OKUDA T., SAKAMOTO K., NISHIMOTO H., DAIMON H., SUGA S., KINOSHITA T. and KAKIZAKI A., *Phys. Rev. B*, **55** (1997) 6762.
[16] HASEGAWA S., MARUYAMA M., HIRATA Y., AHE D. and NAKASHIMA H., *Surf. Sci.*, **405** (1998) L503.
[17] WEITERING H. H., SHI X. and ERWIN S. C., *Phys. Rev. B*, **54** (1996) 10585.
[18] SAKAMOTO K., OKUDA T., NISHIMOTO H., DAIMON H., SUGA S., KINOSHITA T. and KAKIZAKI A., *Phys. Rev. B*, **50** (1994) 1725.
[19] FAN W. C. and IGNATIEV A., *Phys. Rev. B*, **41** (1990) 3592.
[20] WAN K. J., LIN X. F. and NOGAMI J., *Phys. Rev. B*, **46** (1992) 13635.

[21] LOTTERMOSER L., LANDEMARK E., SMILGIES D.-M., NIELSEN M., FEIDENHANS'L R., FALKENBERG G., JOHNSON R. L., GIERER M., SEITSONEN A. P., KLEINE H., BLUDAU H., OVER H., KIM S. K. and JONA F., *Phys. Rev. Lett.*, **80** (1998) 3980.
[22] AN K. S., PARK R. J., KIM J. S., PARK C. Y., KIM C. Y., CHUNG J. W., ABUKAWA T., KONO S., KINOSHITA T., KAKIZAKI A. and ISHII T., *Surf. Sci.*, **337** (1995) L789.
[23] QUINN J. and JONA F., *Surf. Sci.*, **249** (1991) L307.
[24] KUBO O., SARANIN A. A., ZOTOV A. V., RYU J.-T., TANI H., HARADA T., KATAYAMA M., LIFSHITS V. G. and OURA K., *Surf. Sci.*, **415** (1998) L971.
[25] SARANIN A. A., LIFSHITS V. G., IGNATOVICH K. V., BETHGE H., KAYSER R., GOLDBACH H., KLUST A., WOLLSCHLÄGER J. and HENZLER M., *Surf. Sci.*, **448** (2000) 87.
[26] GALLUS O., STAROWICZ P., PILLO TH. and BAER Y., in preparation.
[27] FUKUDA T., *Phys. Rev. B*, **50** (1994) 1969.
[28] LIPSON H. and SINGER K. E., *J. Phys. C*, **7** (1974) 12.
[29] VOIT J., PERFETTI L., ZWICK F., BERGER H., MARGARITONDO G., GRÜNER G., HÖCHST H. and GRIONI M., *Science*, **290** (2000) 501.
[30] PETROVYKH D. Y., ALTMANN K. N., LIN J. L., HIMPSEL F. J. and LEIBSLE F. M., *Surf. Sci.*, **512** (2002) 269.

Publication [3]

P. Starowicz, O. Gallus, Th. Pillo, and Y. Baer, *Size Effects in Photoemission of One-Dimensional Metals*, Physical Review Letters **89**, 256402 (2002).

Size Effects in Photoemission of One-Dimensional Metals

P. Starowicz, O. Gallus, Th. Pillo, and Y. Baer
Physics Institute, University of Neuchâtel, CH-2000 Neuchâtel, Switzerland
(Received 28 May 2002; published 4 December 2002)

High-resolution photoemission spectra of an array of one-dimensional (1D) metallic chains created on Si(335) reveal characteristic features precluding any interpretation within known theoretical models. The origin of this dilemma is attributed to imperfections acting as boundaries in 1D systems. A simple model calculation including a Coulomb shift in the photoemission final state of chain segments yields straight simulations of our spectra and is likely to clarify the confusing situation encountered in this field.

DOI: 10.1103/PhysRevLett.89.256402 PACS numbers: 71.10.Pm, 73.20.At, 73.21.–b, 79.60.Jv

One-dimensional (1D) metals represent a fascinating class of materials expected to show unique properties resulting from the breakdown of the Fermi liquid approach. Tomonaga and Luttinger [1,2] (TL) have first demonstrated in the limit of small energies $\omega = E - E_F$ that only collective spin and charge excitations (spinons and holons) can exist in 1D metals. The momentum-resolved spectral functions $A(\omega, k)$ calculated for reasonable values of the interaction-dependent parameter α show the typical behavior of separated spinons and holons [3]. These two excitations are revealed by two sharp dispersing peaks converging at the Fermi wave vector k_F in a single structure described by the power law $A(\omega, k_F) \sim |\omega|^{\alpha-1}$. The momentum-integrated spectral function close to E_F is also a simple power law $A(\omega) \sim |\omega|^{\alpha}$.

Strictly 1D metallic states are not likely to occur in nature but are approximately realized in highly anisotropic solids or surfaces containing arrays of metallic chains with a very weak mutual interaction. In 1D metallic systems with short range interactions, fluctuations impede phase transitions [4] which can occur only in chain arrays when the transverse interaction dominates the thermal energy. This sets a lower limit to the temperature of the measurements, which are then suffering from thermal broadening in the crucial low-energy range.

The direct observation of the TL predictions with photoemission is a challenging problem. The earliest studies with angle-integrated photoemission have confirmed that quasi-1D metals never show the characteristic Fermi edge of conventional metals [5,6]. The first enthusiasm raised by these results has been toned down by the systematic observation of anomalously large values of $\alpha > 1$ extracted from the slope of the intensity vanishing at E_F. Recent studies exploiting state-of-the-art angular and energy resolutions are puzzling and do not provide more clear-cut observations of the TL predictions: for example, different Bechgaard salts show at $\sim$1 eV a non-dispersing and broad peak followed by a featureless tail down to E_F [7]. In the organic conductor TTF-TCNQ (tetrathiafulvalene-tetracyanoquinodimethane) the dispersing band approaching E_F remains pinned at 200 meV and no feature of the low-energy spectral shape predicted by the TL theory can be discerned [8,9]. A critical analysis of the spectra of $K_{0.3}MoO_3$ and $Li_{0.9}MoO_{17}$ [10] leads to the conclusion that within a few hundred meV's the low-energy line shapes cannot be reconciled with any predicted spectral function. In $(TaSe_4)_2I$, an unexpected gap with a completely flat intensity at E_F could be only tentatively explained with a polaronic model [11]. The systematic impossibility to analyze with any known model the low-energy excitations observed in photoemission spectra of quite different classes of 1D metals suggests that this puzzling problem must originate from some generic mechanism related to the photoemission process itself in this type of samples. On the basis of high-resolution spectra of an artificial array of metallic chains, we show in the present study that Coulomb gaps resulting from the photoexcitation of small metallic aggregates provide a natural interpretation of this situation.

In the present study, the substrate is a Si wafer [p type, B doped, $\rho(300\ \mathrm{K}) = 10\ \Omega\,\mathrm{cm}$] with faces parallel to the crystalline plane (335). After a standard cleaning by flashes at 1250 °C, a precise coverage of 0.28 ML (monolayer) of Au [with respect to the atom concentration of Si(111)] is evaporated onto the substrate and annealed at 780 °C. Sharp LEED patterns reveal a pure (3×1) reconstruction corresponding to a uniform distribution of terraces along the $[1\bar{1}0]$ direction separated by monoatomic steps. This structure is very stable and can be used as a template [12]. Afterwards, about 1 ML of Na is deposited onto this template, heated to 350 °C, and slowly cooled to room temperature. By preferential desorption, the surface is decorated by the Na atoms and the previous (3×1) LEED pattern is very precisely restored and remains stable as a function of temperature. As a consequence of the good matching of the metallic radius of Na to the periodicity of the substrate, one can anticipate that metallic chains are formed along the terraces, as confirmed by the photoemission spectra. The absence of phase transitions in the temperature range of our

measurements points to a negligible interchain coupling supporting the hypothesis of a structure with one Na atom per unit cell. Finally, this structure remains surprisingly stable under UV irradiation even at low temperature. The quality of this sample offers exceptional conditions for studying the low-energy excitations. Linearly p-polarized photons of 21.2 eV have been used for the measurements performed at 14 K with an energy and angular resolution of 5 meV and $\pm 0.5°$, respectively. The base pressure was maintained below 5×10^{-11} mbar during the sample preparation and the measurements.

A collection of angle-resolved spectra for a wave vector variation along the terraces is shown in Fig. 1. The weakly dispersing peak observed around 1.2 eV is tentatively interpreted as an interface state originating from the Au atoms stabilizing the regular step structure of the surface. From 30° another structure located at 0.9 eV emerges and shows a regular dispersion up to 34°. By extrapolation one finds that this peak would cross E_F at 36°, but for angles larger than 34°, the dispersion saturates and the peak dies smoothly without approaching E_F closer than 130 meV. The 1D character of this band originating from the presence of the Na atoms is demonstrated by the lack of dispersion in spectra recorded for $\vec{k}$ perpendicular to the terraces (not shown here). In the spectra of Fig. 1 our high instrumental resolution is exclusively revealed by the sharp intensity onset observed at E_F. In the low-energy range, the absence of any indication of backfolding eliminates an interpretation in terms of a conventional band of an insulator or semimetal. Within the TL framework, the linear behavior observed close to E_F corresponds to an unrealistic large value $\alpha = 2$. This impossibility to interpret our data with any predicted spectral function leads us to the conclusion that the low-energy behavior of the spectra is overwhelmed by some specific mechanism originating from the photoemission process in this class of solids.

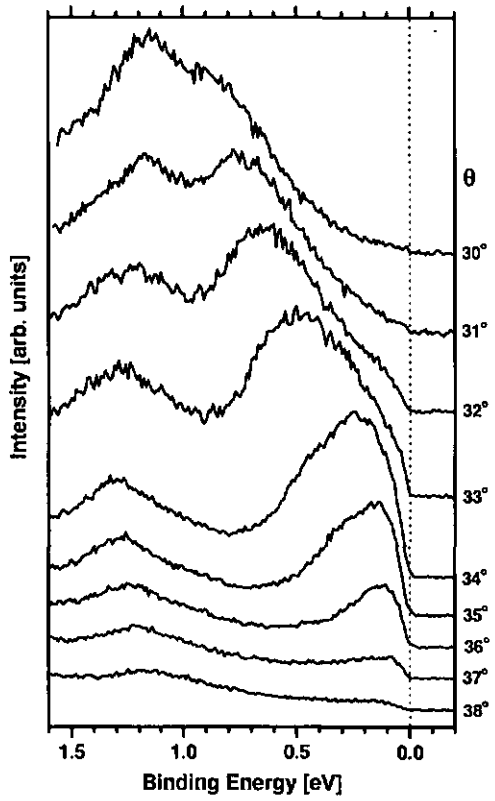

FIG. 1. Angle-resolved photoemission spectra of the one-dimensional band induced by Na atoms on Si(335)-Au. The different angles θ correspond to a variation of the wave vector along the terraces.

Quasi-1D metallic samples consist of a periodic array of nearly independent chains embedded in a poorly conducting medium. These chains are commonly assumed to be sufficiently long to prevent any size effect. In fact, UV photoemission is probing only a few monolayers of sample surfaces, which have been prepared by cleavage or some other artificial procedure generating lattice defects and accumulating impurities. For example, an STM image of the Si(557)-Au surface [13] shows that the mean length of the uninterrupted periodic ranges along the terraces is of the order of 4.5 nm. In 1D systems such imperfections have a crucial importance for the charge transport since they act as strong barriers cutting the chains [14]. Different theories including boundaries in the TL model have been proposed [15–17]. The fact that they are hardly reconciled with experiments has raised the general idea of the model developed below [16,17]. The measured part of the sample is likely to be at best described as a collection of isolated metallic chain segments with some distribution of their length L. These segments have a common Fermi energy in the ground state but the photoemission process leaves them in excited states with a positive charge. As a consequence, the work function of a segment of length L will contain a Coulomb shift $\phi(L)$ resulting from this positive charge. This energy originates from the small size of the probed objects but not specifically from their 1D character and for clusters, L can be generalized as a size parameter. In photoemission, the consequence of this mechanism is that the energy ω observed for a state belonging to an infinite chain will be shifted to $\varepsilon = \omega + \phi(L)$ for a chain of length L. This phenomenon has the same origin as the charging energy observed in the Coulomb blockade. It is established that the ionization potential of isolated spherical clusters shows a typical $1/L$ decrease successfully interpreted within a semiclassical density variational method [18]. However, our surface presents markedly different conditions: the clusters form a regular array of close 1D segments and their mutual screening as well as the dielectric response of the substrate reduces the Coulomb shift. We are not aware of any realistic calculation accounting for this situation, but we can rely on STM data of metallic clusters deposited on TiO_2 [19]. Images and densities of states obtained for individual clusters reveal that their band gaps (2ϕ) as a function of

their size decrease more abruptly than the ionization energy observed for isolated clusters. For this reason we have empirically looked for a function reproducing the general shape of $\phi(L)$ observed with STM for the deposited clusters [19]. With increasing cluster size L, the rather steep variation of ϕ observed in experiment is simulated by multiplying the $1/L$ dependence for free clusters by an exponentially decaying function, which gives $\phi(L) \sim \exp(\frac{-L}{\lambda})/L$ with λ as adjustable attenuation length. We have assumed a Gaussian size distribution $G(L)$ of clusters with mean value $\bar{L}$ and full width at half maximum (FWHM) σ. $G(L)$ can be transformed into a shift distribution $P(\phi)$: $G(L)dL = G[L(\phi)]\frac{dL}{d\phi}d\phi = P(\phi)d\phi$. If the spectral function for $L \to \infty$ is $A(\omega, k)$, the spectrum for the chain distribution is given by $I(\varepsilon, k) = \int_{\omega<\varepsilon} A(\omega, k)P(\varepsilon - \omega)d\omega$. The precise functional dependence of $\phi(L)$ is not very critical and our particular choice is merely justified by the fact that it has the ability to satisfactorily mimic the shifts measured for clusters deposited on TiO_2 [19] and offers the possibility to simulate the low-energy photoemission spectral shapes observed in different 1D systems. In Fig. 2, A and B illustrate typical curves $G(L)$ and $\phi(L)$ used for calculations and curve C illustrates an angle-integrated spectrum computed with the presented Coulomb shift model (CSM) for a conventional metal at $T = 0$ K with a constant $A(\omega)$ below E_F. The Fermi edge is replaced by a sharp onset of the intensity that gradually saturates at higher energies. This shape compares favorably with the angle-integrated spectrum (Fig. 2, curve E) measured for silver clusters deposited on graphite [21]. A quite similar situation occurs in granular Pb films evaporated on an insulator [20] and the typical spectrum from this study reported in Fig. 2 (curve D) is again in convincing agreement with our model calculation. For such samples, the size parameter L depends on the different dimensions, shapes, orientations, and proximities of the clusters. The experimental spectra reported in Fig. 2 correspond to a mean cluster radius of approximately 3 nm [19,21], and it is gratifying to notice that the opening of a gap observed in experiments for smaller clusters [21,20] can be quite naturally reproduced by the model if $\bar{L}$ and σ are reduced. These comparisons with cluster data establish the soundness of the CSM which will be used now to analyze the present spectra.

At k_F, the angle-resolved photoemission spectrum of a metallic band is normally accounting for a sharp state at E_F and a δ function is a good approximation of such a spectral line shape. In Fig. 3, the spectra A and C calculated with the CSM for $A(\omega, k_F) = \delta(\omega)$ have lost the sharp character of the state at E_F which is revealed only by the abruptness of the linear intensity onset. The overall spectral shape is an asymmetric and broad peak with a long tail on the high-energy side. The agreement of the calculated spectrum (A) with our measured spectrum at k_F (~36°) shown in Fig. 3 (B) is striking and, within the TL model, the existence of a sharp state at E_F is consistent with $\alpha < 1$. The same analysis of our previous spectrum at k_F of Si(557)-Au [22] is also shown in the same figure. The narrowing and shift toward E_F of the spectrum (D) can be simply simulated by a small increase of $\bar{L}$ and σ as shown by curve C. The agreement between the model calculation C and the experimental spectrum D is again convincing and confirms that a previous interpretation of this low-energy edge as a Fermi step of a conventional metal [13] can be discarded. However, one must be aware that a finite chain length induces a wave vector uncertainty Δk, but the resulting broadening is very unlikely to provide a major contribution to the line shapes. This assumption relies on the fact that in a Luttinger liquid, a partial integration of $A(\omega, k)$ over Δk can result in a linear intensity onset only for $\alpha = 1$. This mechanism is not credible since the observation of the same onset behavior in quite different 1D systems (organic [8], inorganic [10], surface states [22]) would imply that they

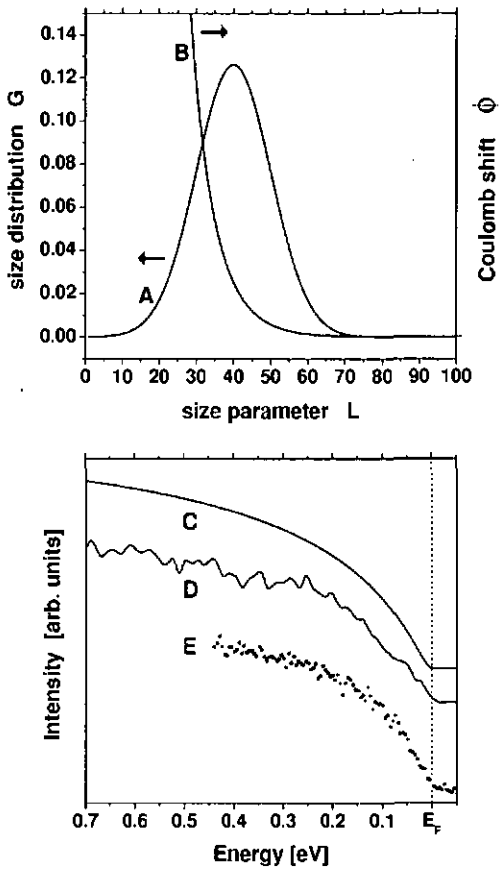

FIG. 2. (A) Gaussian distribution curve $G(L)$ of the clusters (chains) versus their size parameter (length) L. If the mean size parameter is $\bar{L}$, the FWHM is given by $\sigma = 0.59\bar{L}$. (B) Coulomb shift $\phi(L)$ for $\lambda = 0.20\bar{L}$ (see text). (C) Angle-integrated photoemission spectrum of a constant metallic density of states calculated with the CSM defined by $G(L)$ and $\phi(L)$. (D) Angle-integrated photoemission spectrum of a 6 Å granular film of Pb evaporated on Ta oxide covered with 2 ML of Ge [20]. (E) Angle-integrated photoemission spectrum of Ag clusters containing 4×10^3 atoms on graphite [21].

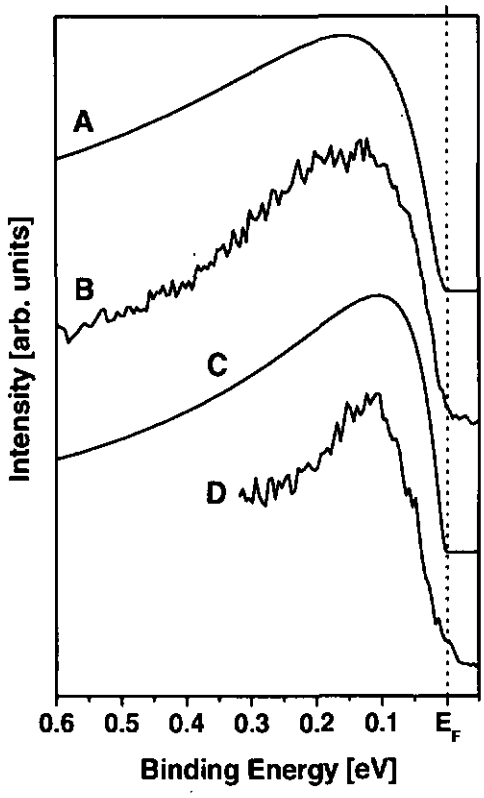

FIG. 3. Curves A and C are simulations with the CSM of angle-resolved spectra originating from a spectral function assumed to be a delta function at E_F. The parameters of curve A are $\sigma = 0.47\bar{L}$ and $\lambda = 0.2\bar{L}$ (see Fig. 2). For curve C, σ and $\bar{L}$ have been increased by approximately 5% while the absolute value of λ remains the same as in simulation A. The spectra B and D are angle-resolved photoemission measurements at k_F, B is a spectrum at $\theta = 36°$ from the present study, and D is reproduced from Ref. [22] for Si(557)-Au.

are all characterized by the same anomalously large value of the interaction-dependent parameter α.

As in other 1D systems [8,10], the overall line shapes of our spectra shown in Fig. 1 are complex, but we refrain from attempting a detailed analysis here. Our aim is solely to show that our data suggest the existence of a particular mechanism originating from the photoemission process in this type of sample. The validity of the proposed CSM is not limited to 1D systems showing a linear intensity onset and to clusters, but it has the virtue to offer a qualitative explanation of other strange aspects observed in the low-energy spectral range of 1D metals. The mean chain length $\bar{L}$ determines the position of the peaks at k_F and when $\bar{L}$ becomes markedly short, the peak moves away from E_F where a gap gradually opens with no discernible intensity. Hence, this simulation offers an alternative explanation to the polaronic model proposed for interpreting the gap in $(TaSe_4)_2I$ [11]. Finally, in highly disordered surfaces, $\bar{L}$ becomes so small that the dispersion is destroyed and the spectra merely show a broad peak at ~1 eV [7]. The interpretation in terms of spin-charge separation of the spectra obtained for the surface Si(557)-Au [22] is not settled [13], but it is strengthened by the fact that in this system the peak at k_F has the closest position relative to E_F (~ 100 meV) ever observed in 1D systems. In accordance with the CSM, the two individual peaks are resolved only when their separation exceeds 100 meV.

The assumption of Coulomb shifts in the photoemission spectra of 1D metals provides a general and credible explanation of the involved situation which has obscured the interpretation of the data over more than one decade. The CSM sets a serious limitation to the application of this method to small isolated particles, but the situation is not hopeless for 1D metals. One can anticipate that efforts to produce better-characterized surfaces containing longer chains will be rewarded with unambiguous observations of the low-energy spectral functions predicted by the TL model.

This work has been supported by the Swiss National Scientific Foundation.

[1] S. Tomonaga, Prog. Theor. Phys. **5**, 544 (1950).
[2] J. M. Luttinger, J. Math. Phys. (N.Y.) **4**, 1154 (1963).
[3] J. Voit, J. Electron Spectrosc. Relat. Phenom. **117**, 469 (2001).
[4] D. L. Landau and E. M. Lifchitz, *Physique Statistique* (Mir Publishing Company, Moscow, 1967), p. 576.
[5] B. Dardel *et al.*, Phys. Rev. Lett. **67**, 3144 (1991).
[6] B. Dardel *et al.*, Europhys. Lett. **24**, 687 (1993).
[7] F. Zwick *et al.*, Phys. Rev. Lett. **79**, 3982 (1997).
[8] F. Zwick *et al.*, Phys. Rev. Lett. **81**, 2974 (1998).
[9] R. Claessen *et al.*, Phys. Rev. Lett. **88**, 096402 (2002).
[10] G.H. Gweon *et al.*, J. Electron Spectrosc. Relat. Phenom. **117**, 481 (2001).
[11] L. Perfetti *et al.*, Phys. Rev. Lett. **87**, 216404 (2001).
[12] M. Jalochowski and E. Bauer, Prog. Surf. Sci. **67**, 79 (2001).
[13] R. Losio *et al.*, Phys. Rev. Lett. **86**, 4632 (2001).
[14] V. Meden, W. Metzner, U. Schollwöck, and K. Schönhammer, J. Low Temp. Phys. **126**, 1147 (2002).
[15] A. E. Mattsson, S. Eggert, and H. Johannesson, Phys. Rev. B **56**, 15 615 (1997).
[16] J. Voit, Y. P. Wang, and M. Grioni, Phys. Rev. B **61**, 7930 (2000).
[17] V. Meden *et al.*, Eur. Phys. J. B **16**, 631 (2000).
[18] M. Seidl, K.-H. Meiwes-Broer, and M. Brack, J. Chem. Phys. **95**, 1295 (1991).
[19] M. Valden, X. Lai, and D.W. Goodman, Science **281**, 1647 (1998).
[20] D. J. Huang, G. Reisfeld, and M. Strongin, Phys. Rev. B **55**, R1977 (1997).
[21] H. Hövel, B. Grimm, M. Pollmann, and B. Reihl, Phys. Rev. Lett. **81**, 4608 (1998).
[22] P. Segovia, D. Purdie, M. Hengsberger, and Y. Baer, Nature (London) **402**, 504 (1999).